



A Necroptosis-Related lncRNA-Based Signature to Predict Prognosis and Probe Molecular Characteristics of Stomach Adenocarcinoma

Lianghua Luo^{1†}, Leyan Li^{2†}, Li Liu¹, Zongfeng Feng¹, Qingwen Zeng¹, Xufeng Shu¹, Yi Cao¹ and Zhengrong Li^{1*}

¹Department of Gastrointestinal Surgery, The First Affiliated Hospital, Nanchang University, Nanchang, China, ²Queen Mary School, Medical Department of Nanchang University, Nanchang, China

OPEN ACCESS

Edited by:

Jinhui Liu,
Nanjing Medical University, China

Reviewed by:

Chuanpeng Dong,
Purdue University Indianapolis,
United States
Feng Jiang,
Fudan University, China

*Correspondence:

Zhengrong Li
lzh13@foxmail.com

[†]These authors have contributed
equally to this work

Specialty section:

This article was submitted to
RNA,
a section of the journal
Frontiers in Genetics

Received: 19 December 2021

Accepted: 11 February 2022

Published: 07 March 2022

Citation:

Luo L, Li L, Liu L, Feng Z, Zeng Q,
Shu X, Cao Y and Li Z (2022) A
Necroptosis-Related lncRNA-Based
Signature to Predict Prognosis and
Probe Molecular Characteristics of
Stomach Adenocarcinoma.
Front. Genet. 13:833928.
doi: 10.3389/fgene.2022.833928

Background: As a caspase-independent type of cell death, necroptosis plays a significant role in the initiation, and progression of gastric cancer (GC). Numerous studies have confirmed that long non-coding RNAs (lncRNAs) are closely related to the prognosis of patients with GC. However, the relationship between necroptosis and lncRNAs in GC remains unclear.

Methods: The molecular profiling data (RNA-sequencing and somatic mutation data) and clinical information of patients with stomach adenocarcinoma (STAD) were retrieved from The Cancer Genome Atlas (TCGA) database. Pearson correlation analysis was conducted to identify the necroptosis-related lncRNAs (NRLs). Subsequently, univariate Cox regression and LASSO-Cox regression were conducted to establish a 12-NRLs signature in the training set and validate it in the testing set. Finally, the prognostic power of the 12-NRLs signature was appraised via survival analysis, nomogram, Cox regression, clinicopathological characteristics correlation analysis, and the receiver operating characteristic (ROC) curve. Furthermore, correlations between the signature risk score (RS) and immune cell infiltration, immune checkpoint molecules, somatic gene mutations, and anticancer drug sensitivity were analyzed.

Results: In the present study, a 12-NRLs signature comprising REPIN1-AS1, UBL7-AS1, LINC00460, LINC02773, CHROMR, LINC01094, FLNB-AS1, ITFG1-AS1, LASTR, PINK1-AS, LINC01638, and PVT1 was developed to improve the prognosis prediction of STAD patients. Unsupervised methods, including principal component analysis and t-distributed stochastic neighbor embedding, confirmed the capability of the present

Abbreviations: GC: Gastric cancer; lncRNAs: Long non-coding RNAs; NRLs: Necroptosis-related lncRNAs; STAD: Stomach adenocarcinoma; RNA-seq: RNA-sequencing; TCGA: The Cancer Genome Atlas; LASSO: The least absolute shrinkage and selection operator; ROC: Receiver operating characteristic; K-M: Kaplan-Meier; DCA: decision curve analysis; RIPK1/RIPK3: Receptor Interacting Protein Kinase1/3; MLKL: Mixed Lineage Kinase Domain Like Pseudokinase; AML: acute myeloid leukemia; lncRNA: Long non-coding RNA; ncRNAs: non-protein coding RNAs; RS: Risk score; OS: Overall survival; AUC: areas under the curve; TME: Tumor microenvironment; ssGSEA: Single sample Gene Set Enrichment analysis; GSEA: Gene Set Enrichment Analysis; KEGG: Kyoto Encyclopedia of Genes and Genomes; IC50: Half maximal inhibitory concentration; HR: Hazard ratio; Tregs: T cells regulatory; TMB: Tumor mutation burden; HNSCC: Head and neck squamous cell carcinoma; EMT: Epithelial-mesenchymal transition; TNBC: triple-negative breast cancer; TIDE: Tumor Immune Dysfunction and Exclusion; ICI: Immune checkpoint inhibitor; FPKM: Fragments Per Kilobase Million.

signature to separate samples with RS. Kaplan-Meier and ROC curves revealed that the signature had an acceptable predictive potency in the TCGA training and testing sets. Cox regression and stratified survival analysis indicated that the 12-NRLs signature were risk factors independent of various clinical parameters. Additionally, immune cell infiltration, immune checkpoint molecules, somatic gene mutations, and half-inhibitory concentration differed significantly among different risk subtypes, which implied that the signature could assess the clinical efficacy of chemotherapy and immunotherapy.

Conclusion: This 12-NRLs risk signature may help assess the prognosis and molecular features of patients with STAD and improve treatment modalities, thus can be further applied clinically.

Keywords: necroptosis, lncRNA, signature, prognosis, molecular characteristics, stomach adenocarcinoma

INTRODUCTION

Gastric cancer (GC) is a highly aggressive and extremely heterogeneous malignancy that causes high morbidity and mortality globally. According to *Global Cancer Report 2020*, GC accounts for over 1 million new cases and nearly 760,000 deaths worldwide each year (Sung et al., 2021). The most general histological subtype of GC is stomach adenocarcinoma (STAD), which is highly fatal. Despite substantial advances in surgical procedures, adjuvant treatments, and examination techniques over the past decades, the prognosis of patients with STAD remains poor, especially for those in the advanced stage with a 5-years survival rate below 20% (Ferlay et al., 2019; Tan, 2019). Due to differences in genetic characteristics, STAD patients with similar tumor histology, and the same pathological stage may have completely distinct oncologic outcomes. Hence, exploring novel efficient biomarkers and therapeutic approaches is crucial to improving the prognosis and treatment of STAD patients.

Necroptosis is a new type of cell death mediated by Receptor Interacting Protein Kinase1/3 (RIPK1/RIPK3) and executed by Mixed Lineage Kinase Domain Like Pseudokinase (MLKL) (Declercq et al., 2009; Marshall and Baines, 2014). The exact effect of necroptosis in tumors is complex and controversial. On the one hand, necroptosis suppresses tumors during cancer initiation and metastasis by inhibiting osteosarcoma, colorectal cancer, acute myeloid leukemia (AML), and breast cancer (Fu et al., 2013; Nagues et al., 2014; Feng et al., 2015; Koo et al., 2015). On the other hand, necroptosis has been demonstrated to promote tumor cell growth and tumor metastasis. *In vivo*, different RIPK1 inhibitors can prevent tumor growth and limit metastasis (Strilic et al., 2016; Li et al., 2018). In a mouse breast cancer model, the absence and depletion of MLKL blocked metastasis of breast cancer cells to the lung (Jiao et al., 2018).

Long non-coding RNA (lncRNA) is a class of non-protein-coding RNAs (ncRNAs) with a length of over 200 nucleotides but several special functions, such as mRNA splicing, transcription regulation, and mRNA post-transcriptional regulation (Guttman and Rinn, 2012; Zuo et al., 2021). lncRNAs have been proved closely related to tumor development, metastasis, and cancer immunity, and their good molecular stability could make them new potential prognostic biomarkers in cancer patients (Huarte,

2015; Bhan et al., 2017; Denaro et al., 2019; Statello et al., 2021). Therefore, further elucidating the relationship between necroptosis-related lncRNAs (NRLs) and STAD is essential for exploring novel therapeutic targets for STAD and improving patient prognosis.

In this study, NRLs were mined from TCGA-STAD transcript data via Pearson correlation analysis. Then, a 12-NRLs signature for predicting the survival of STAD patients was proposed through univariate analysis and LASSO regression analysis. Moreover, molecular characteristics exploration based on the 12-NRLs signature was crucial to supplying a robust theoretical basis for applying immunotherapy and chemotherapy to STAD patients.

MATERIALS AND METHODS

Data Collection

The clinical information and RNA-sequencing (RNA-seq) profile of STAD patients were retrieved from the TCGA platform (<https://portal.gdc.cancer.gov/repository>, up to 13 September 2021). The RNA-seq data from the TCGA database had been normalized to Fragments Per Kilobase Million (FPKM) format for subsequent data analysis. To improve research accuracy, only samples with integral clinicopathological information were included for analysis after pre-processing based on the Perl programming language (version Strawberry-Perl-5.30.0.1; <https://www.perl.org>). Subsequently, all patient information was randomly allocated into the training and the testing sets via the “caret” package in R (version 4.1.0, <https://www.r-project.org/>). A total of 39 necroptosis-related genes was acquired by searching published studies (Hanson, 2016; Chen et al., 2019; Molnár et al., 2019; Zhu et al., 2019; Liu et al., 2021). In addition, the mutation data of STAD samples were downloaded in MAF format from the TCGA database.

Identification of NRLs in STAD

Using the GTF annotation files of human lncRNAs retrieved from the GENCODE (<https://www.encodegenes.org/>, up to 13 September 2021) website, 4,497 lncRNAs were identified from the TCGA-STAD RNA-seq data. Subsequently, the co-expression relationships between necroptosis-related genes and all lncRNAs in STAD samples were examined by Pearson correlation analysis,

and those lncRNAs were considered significantly associated with necroptotic mRNAs. $|\text{Coefficient}| > 0.3$ and $p\text{-value} < 0.01$ were considered as the cutoff.

Establishment of the Necroptosis-Related lncRNA-mRNA Co-expression and Protein-Protein Interaction Network

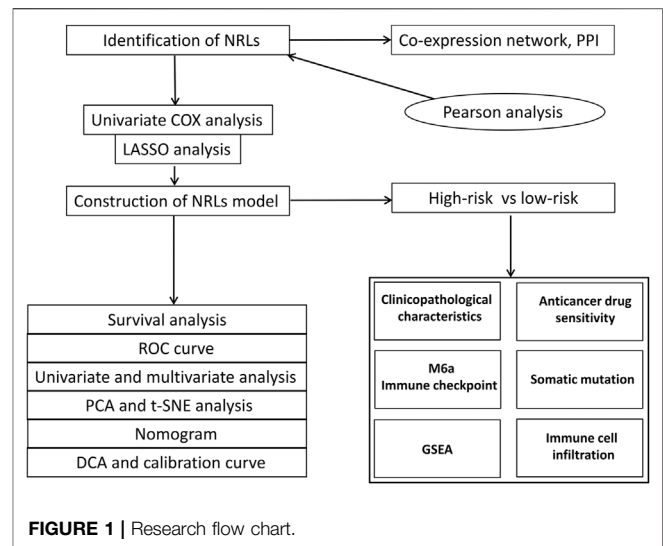
To demonstrate the mutually regulated connection between NLRs and corresponding target mRNAs, we visualized the lncRNA-mRNA network using the “igraph” package in R. Additionally, the necroptosis-related genes regulated by candidate lncRNAs were uploaded to the STRING (version 11.5, <https://www.string-db.org/>) website to build the protein-protein interaction (PPI) network.

Construction and Verification of the NRLs Signature of STAD

Univariate Cox proportional regression analysis was applied to determine the prognosis-related lncRNAs ($p < 0.05$) in TCGA-STAD. Then, the LASSO Cox regression algorithm was adopted to ascertain the optimal panel of prognostic lncRNAs and establish an optimal signature. Next, each STAD patient's survival risk score (RS) was calculated based on the standardized expression levels of NRLs and the corresponding regression coefficients derived from the LASSO regression analysis. The calculation is as follows: $RS = \sum_{i=1}^n \text{Coef}(i) \times x(i)$, where $\text{Coef}(i)$ and $x(i)$ represent the coefficient and the standardized expression levels of each NRLs, respectively. The median RS of the training set was utilized as the demarcation point to categorize all included STAD samples into the low-risk or high-risk subsets. Kaplan-Meier (K-M) curves were adopted to contrast the overall survival (OS) of the high-risk and low-risk subsets in the training and testing sets using the “survival” package. The time-dependent ROC curves were used to evaluate survival prediction, and areas under the ROC curve (AUC) were calculated to assess the predictive accuracy and specificity of the NRLs signature.

Nomogram Establishment and the Correlation Between the Prognostic Signature and Clinicopathological Characteristics

In order to verify the independence of the NRLs signature, univariate analysis and multivariate Cox regression analysis were conducted to evaluate the relationship between clinical features or the NRLs signature with OS, especially to study whether the NRLs signature could be considered a hazard element independent of other clinicopathological factors, such as gender, age, grade, stage, and TNM stage for STAD patients. A stratified survival analysis based on different clinicopathological features was conducted to investigate the applicability of the NRLs-based signature. A nomogram considering independent prognostic factors was developed to predict the 1-, 3-, and 5-years OS rates of STAD patients via the “rms” package. In addition, the calibration curves were drawn to compare the consistency



between the predicted 1-, 3-, and 5-years survival probability based on the nomogram and the actual observations. Finally, the decision curve analysis (DCA) curve was plotted to appraise the clinical effect of the nomogram by calculating the net benefits of a series of risk threshold probabilities using the “rmda” package.

Immune Cell Infiltration Analysis

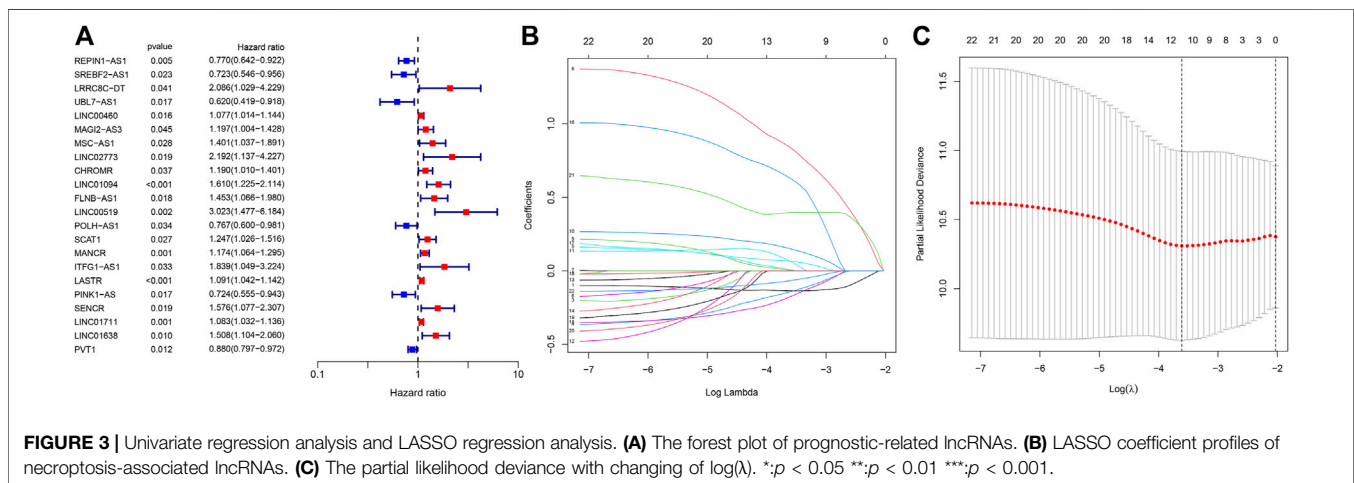
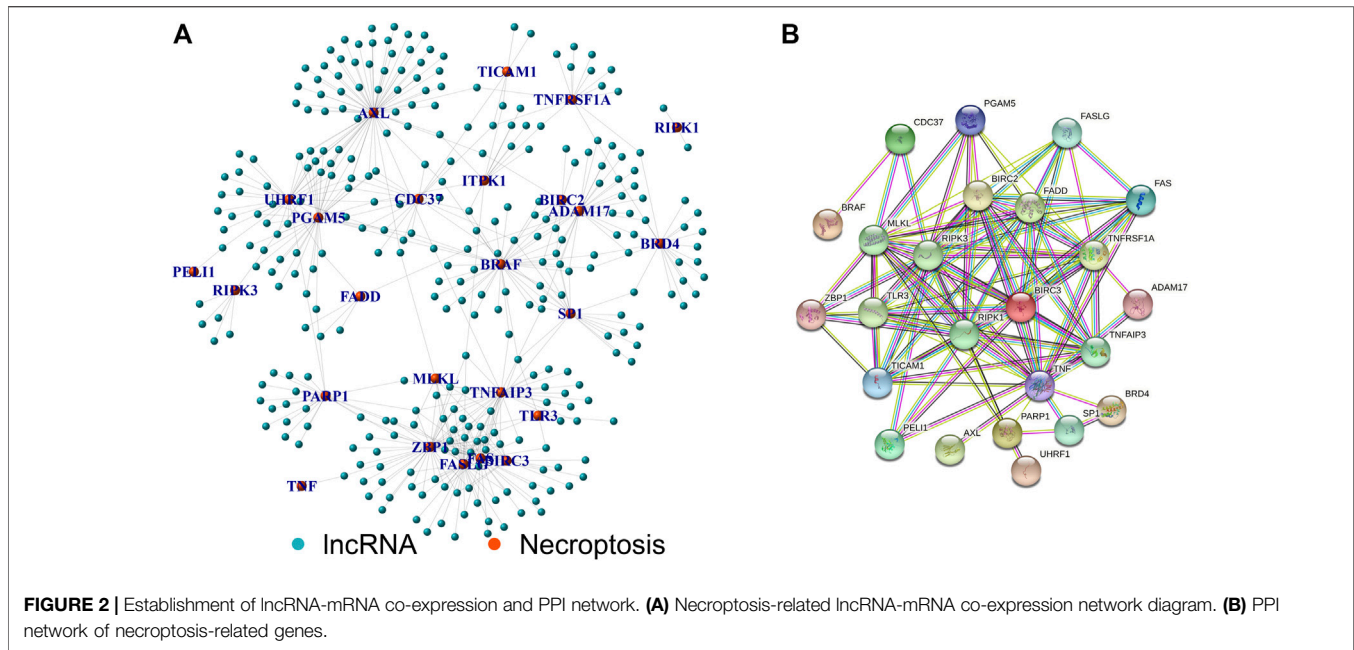
The components of the immune and stromal cells in the tumor microenvironment (TME) of each STAD sample were computed to verify the differences of microenvironment features between unequal risk groups using the ESTIMATE algorithm. The “CIBERSORT” package was adopted to extract the relative proportions of 22 types of human infiltrated immune cells, which could reveal the correlation between the risk signature and immune-cell characteristics. Additionally, the enrichment levels of 29 immune-related functions between the two sets were evaluated by Single sample Gene Set Enrichment Analysis (ssGSEA) scores.

Pathway Enrichment Analysis

In order to clarify the differences of enriched pathways between the low-risk and high-risk subsets, the Gene Set Enrichment Analysis (GSEA) software (version 4.10) was utilized to carry out the Kyoto Encyclopedia of Genes and Genomes (KEGG) pathway enrichment analysis.

Significance of the NRLs-Based Signature in Chemotherapy and Immunotherapy

In order to predict the response of STAD patients in the two different risk subsets to chemotherapy drugs, the “pRRophetic” package was used to assess the half-maximal inhibitory concentration (IC50) of 20 ordinary chemotherapy drugs highly recommended by the 8th American Joint Committee on Cancer (AJCC) guidelines, such as Paclitaxel, Cisplatin, and Imatinib. The differences in IC50 values between the high-risk and low-risk subsets were analyzed by Wilcoxon signed-rank test. The discrepancies of 5 immune checkpoint blockade-related molecules between low-risk and



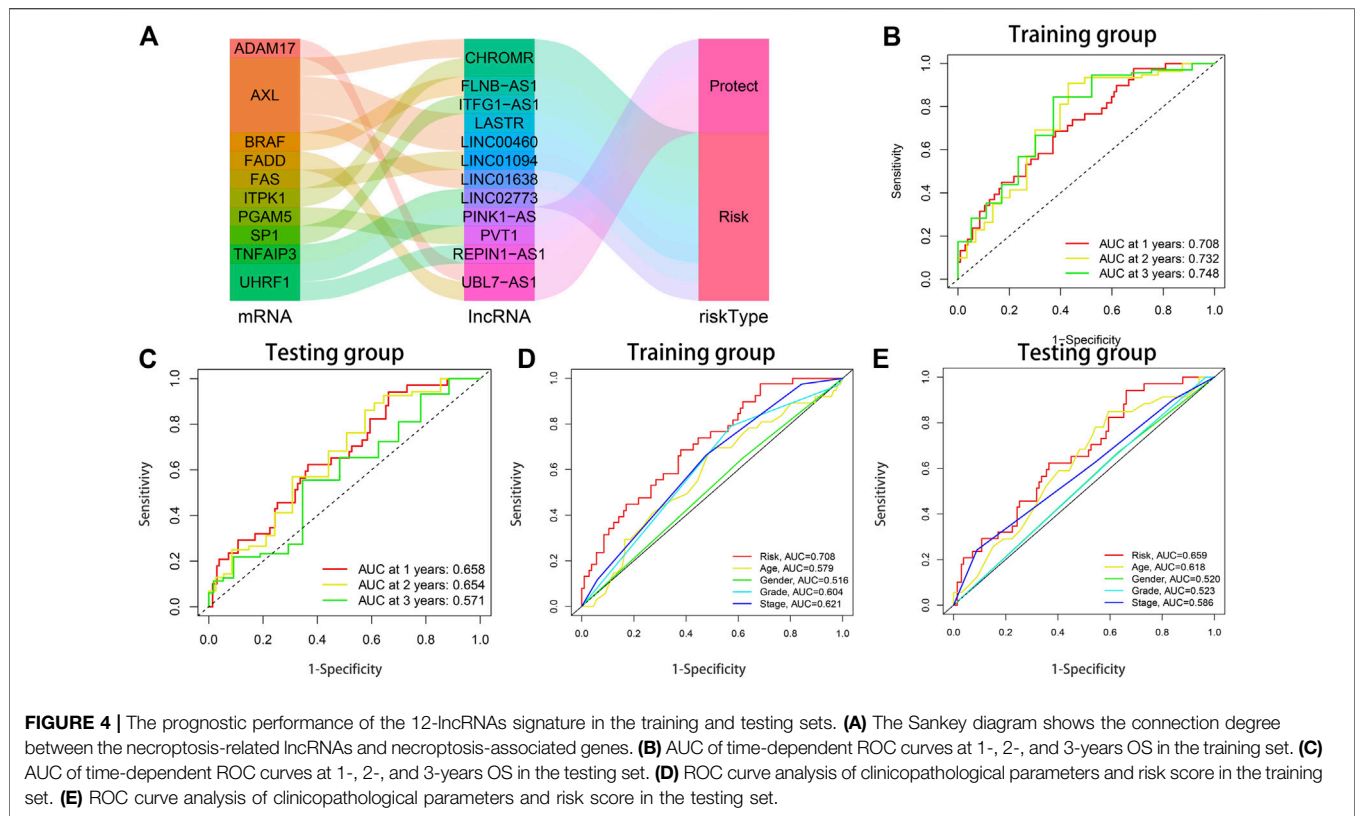
high-risk subsets were examined to appraise the predictive effect of the signature for STAD immunotherapy. The file of Tumor Immune Dysfunction and Exclusion (TIDE) score, T cell dysfunction score, and T cell exclusion score was retrieved from the TIDE website (<http://tide.dfci.harvard.edu>). To estimate the clinical response to immune checkpoint inhibitor (ICI) therapy for STAD patients, TIDE analysis was conducted to predict the potential effect of immunotherapy in different risk subsets.

RESULTS

Identification of NRLs in STAD

Figure 1 shows the flow chart of the research scheme. The transcriptome RNA-seq and clinical data of 407 STAD

patients were collected from the TCGA database, which contained 375 samples of GC tissues and 32 samples of normal gastric tissues. Moreover, 368 samples with complete clinical information were picked out for the following analysis. According to the GTF annotation file of human lncRNAs, 4,497 lncRNAs were identified in TCGA-STAD gene expression files. A total of 39 necroptosis-related genes are exhibited in **Supplementary Table S1**, and 305 lncRNAs were ultimately selected as necroptosis-related lncRNAs. An mRNA-lncRNA co-expression network based on the Pearson correlation analytical results was established to determine the potential effects of NRLs (**Figure 2A**). A PPI network was also established to investigate the connection of these necroptosis-related genes using the STRING database (**Figure 2B**).

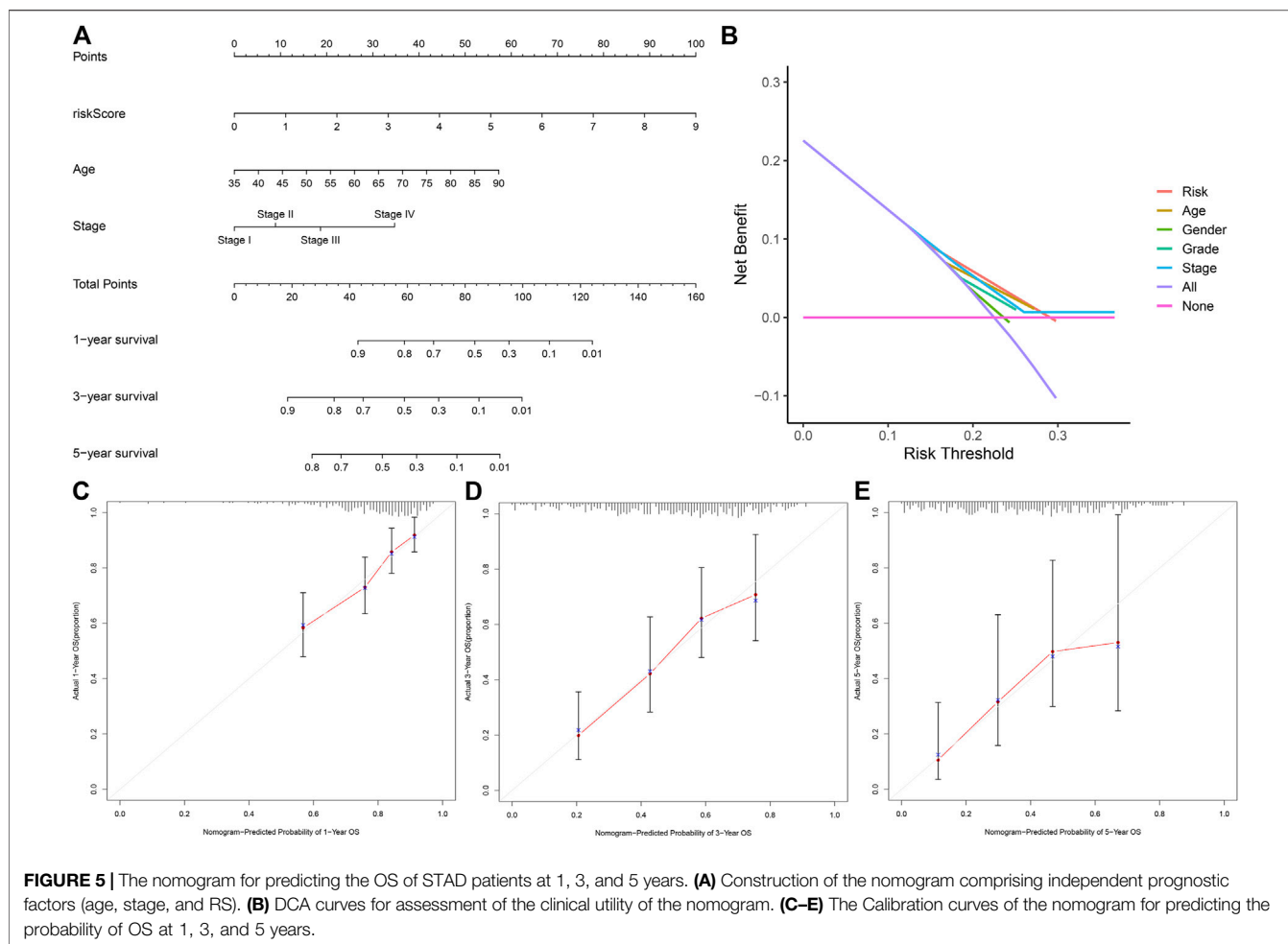


Construction of the NRLs Prognostic Signature

The 368 STAD samples with lncRNAs expression data and integral survival information from the TCGA database were applied to determine the relationship between NRLs and prognosis. An RS-based prognostic signature was built for the final prognostic prediction. Firstly, univariate Cox proportional hazard regression analysis was employed to initially screen 22 lncRNAs associated with the OS of STAD patients from the 305 NRLs ($p < 0.05$, **Figure 3A**; **Supplementary Table S2**). Then, LASSO Cox regression analysis was conducted using the training set to acquire the lncRNAs with the highest prognostic value via the “glmnet” package (**Figures 3B,C**). Finally, 12 lncRNAs were selected for building the optimal prognostic signature of necroptosis-associated lncRNAs, including 8 risk lncRNAs, namely, LINC00460, LINC02773, CHROMR, LINC01094, FLNB-AS1, ITFG1-AS1, LASTR, and LINC01638, and 4 protective lncRNAs, namely, REPIN1-AS1, UBL7-AS1, PINK1-AS, and PVT1. Based on the expression levels of the 12 lncRNAs and the corresponding weighted coefficients, the RS of STAD patients were calculated according to the following formula: $RS = (-0.135,699 \times REPIN1-AS1) + (-0.143,332 \times UBL7-AS1) + (0.065476 \times LINC00460) + (0.840948 \times LINC02773) + (0.003634 \times CHROMR) + (0.150664 \times LINC01094) + (0.065846 \times FLNB-AS1) + (0.632154 \times ITFG1-AS1) + (0.006577 \times LASTR) + (-0.177349 \times PINK1-AS) + (0.396460 \times LINC01638) + (-0.067393 \times PVT1)$ (**Supplementary Table S4**).

Assessment of the 12-NRLs Prognostic Signatures

The 368 STAD samples were randomly allocated into either the training set ($n = 184$) or the testing set ($n = 184$) at a ratio of 1:1. According to the equation above, the clinical RS of each STAD patient was calculated. The median RS of the training set was utilized as the cut-off value to assort both the training and testing sets into the low-risk and high-risk subsets. As exhibited in the scatterplot and risk curve, death cases increase significantly with higher RS (**Supplementary Figure S1A–D**). Heatmaps were drawn to show the expression outlines of the 12 NRLs in the high-risk and low-risk subsets. Among them, 8 risk lncRNAs were significantly upregulated in the high-risk subset, while 4 protective lncRNAs were significantly downregulated (**Supplementary Figure S1E, F**). The K-M curves revealed that the OS of patients with a low RS was significantly longer than those with a high RS (training set: $p < 0.001$; testing set: $p = 0.011$) (**Supplementary Figure S1G, H**). The Sankey diagram not only fully showed the interaction of necroptosis-related lncRNAs and necroptosis-associated genes, but also further illustrated the association between the 12-NRLs risk signature and the OS of STAD patients (**Figure 4A**). The ROC curve was used to assess the prediction performance of the risk signature for the OS of STAD patients. The AUC values of 1, 2, and 3 years for the training and testing sets reached 0.708, 0.732, 0.748, and 0.658, 0.654, 0.571, respectively. Compared with other clinicopathological features, the AUC of RS was the highest



(training set: AUC = 0.708; testing set: AUC = 0.659) (Figures 4B–E). The results indicate that the 12-NRLs signature can prove valuable for patients with STAD.

Establishment and Assessment of the Prognostic Nomogram Based on the 12-NRLs Signature

In order to investigate whether the 12-NRLs signature is an independent prognostic predictor for patients with STAD, Cox regression analysis was carried out. According to univariate Cox regression analysis, RS ($p < 0.001$), stage ($p < 0.001$), and age ($p = 0.002$) were significantly correlated with the OS of STAD patients (Supplementary Figures S2A,B). Moreover, multivariate Cox regression further demonstrated that RS ($p < 0.001$; hazard ratio (HR) = 1.665), stage ($p < 0.001$; HR = 1.694), and age ($p < 0.001$; HR = 1.048) were independent risk factors affecting the prognosis of patients with STAD (Supplementary Figures S2C,D). In order to transform the lncRNAs signature into clinical utility, a nomogram involving the independent risk factors (stage, age, RS) was created to estimate and quantify the survival probability of STAD patients after 1, 3, and 5 years (Figure 5A). Additionally, the calibration curves were plotted to verify the predictive

capability of the nomogram, the results of which suggested the optimal concordance between the predicted survival probability based on the nomogram and the practical observations (Figures 5C–E). Finally, the DCA curve further confirmed that the nomogram based on the 12-NRLs signature had great clinical applicability in estimating the OS of patients with STAD (Figure 5B).

Correlation Between the 12-NRLs Prognostic Signature and Clinicopathological Parameters

A Chi-square test was performed to investigate the associations between the 12-NRLs prognostic signature and clinicopathological parameters. The resulting heatmap revealed that the tumor stage ($p < 0.05$), stage M ($p < 0.05$), stage T ($p < 0.05$), and the histological grade ($p < 0.001$) were significantly different in the high-risk and low-risk subsets (Supplementary Figure S3A). Stratified survival analysis was performed to demonstrate the broad applicability of the signature using the following clinicopathological features (age, gender, grade, stage T, stage N, and stage M) (Supplementary Figures S3B–H), which indicated that in the subsets of males and females, >65 years old

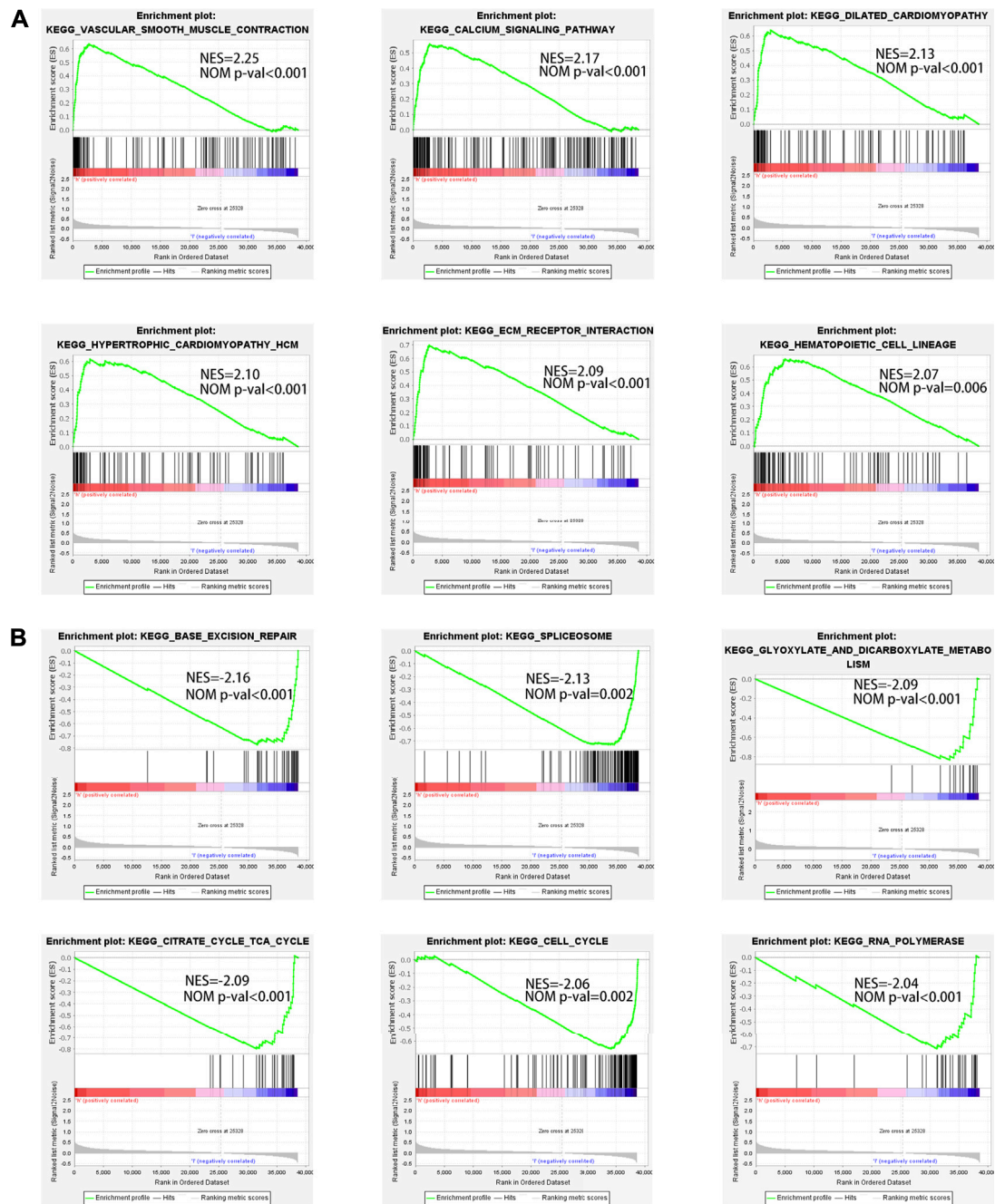


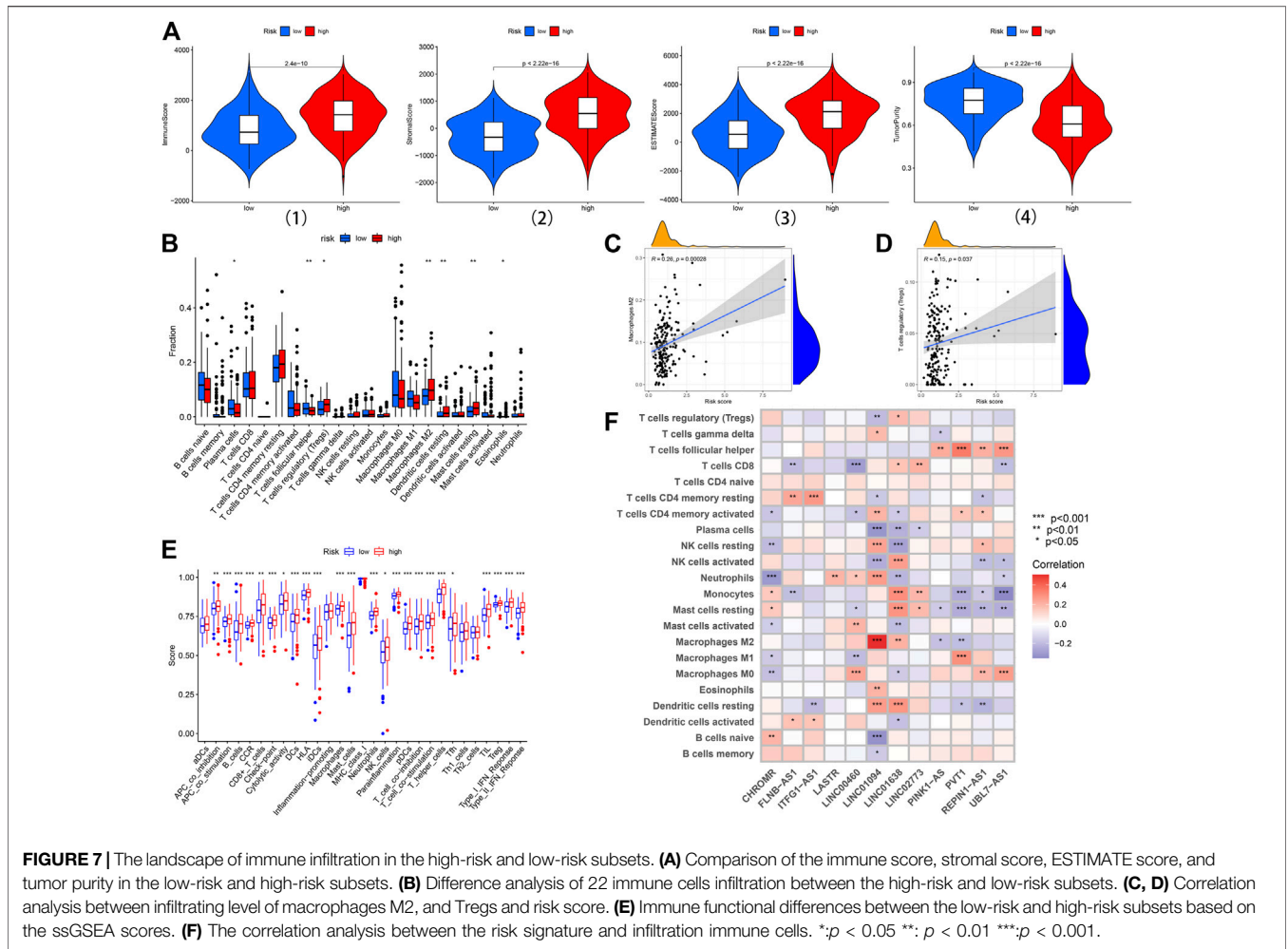
FIGURE 6 | The enriched pathways in high-risk and low-risk subsets obtained using the 12-NRLs signature. **(A)** Top 6 significantly enriched KEGG pathways in the high-risk subset. **(B)** Top 6 significantly enriched KEGG pathways in the low-risk subset.

and ≤ 65 years old, G1-2 and G3, N 1-3, III-IV, M0, and T 3-4, the OS of patients in the high-risk subset was significantly poorer than those in the low-risk subset. Briefly, all these results illustrate that the signature has good applicability in predicting prognosis.

Pathway Enrichment Analysis

In order to elucidate the differences of enriched pathways between the low-risk and high-risk subsets, GSEA was adopted

for KEGG pathway enrichment analysis. The results revealed that the top 6 pathways substantially enriched in the high-risk subset were vascular smooth muscle contraction, hypertrophic cardiomyopathy HCM, dilated cardiomyopathy, ECM receptor interaction, calcium signaling pathway, and hematopoietic cell lineage (Figure 6A). Base excision repair, glyoxylate and dicarboxylate metabolism, spliceosome, citrate cycle TCA cycle, cell cycle, and RNA

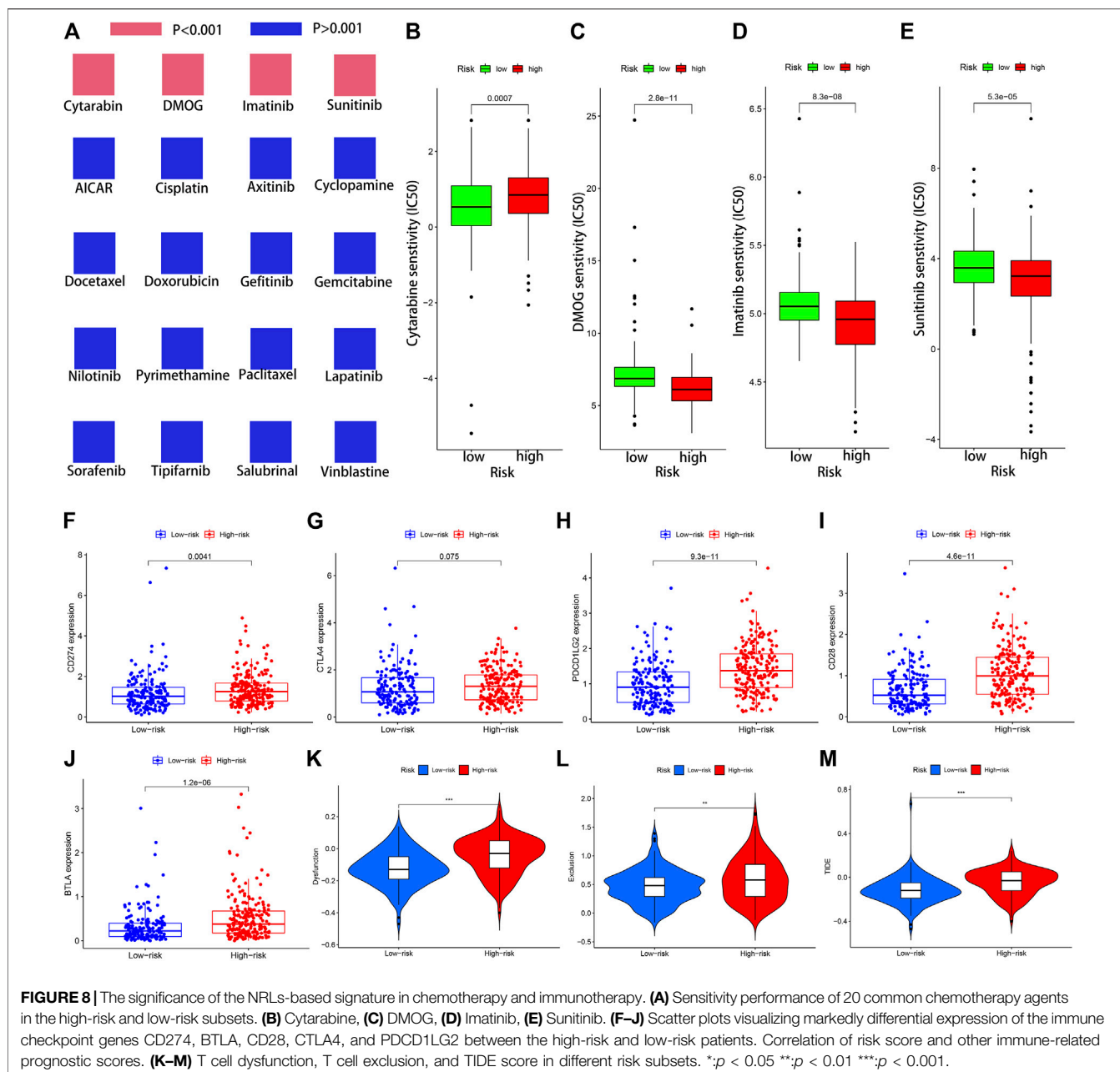


polymerase were markedly enriched in the low-risk subset (Figure 6B).

The Characteristics of TME and Immune Cell Infiltration Between the High-Risk and Low-Risk Subsets

In general, TME was composed of the tumor, stromal, and immune cells. TME scores were applied to measure the differences in the extent of infiltrating stromal and immune cells between the low-risk and high-risk subsets via the “ESTIMATE” package. Samples in the high-risk subset had higher immune, stromal, and estimate scores and lower levels of tumor purity (Figure 7A). In order to further understand the significant difference of TME in different risk subsets, the relative expressions of 22 types of common infiltrated immune cells were calculated and compared between the two groups. The results revealed that T cells regulatory (Tregs), macrophages M2, eosinophils, dendritic cells resting, and mast cells resting were significantly upregulated in the high-risk subset; the expression of T cells follicular helper and plasma cells were significantly

upregulated in the low-risk subset (Figure 7B). Notably, the infiltrated level of immune-suppressive macrophages M2 (Cor = 0.26, $p = 0.00028$) and Tregs (Cor = 0.15, $p = 0.037$) was positively correlated with RS, indicating that the poor prognosis of patients in the high-risk subset may be partly due to the immunosuppressive microenvironment (Figures 7C,D). Furthermore, ssGSEA analysis was carried out to assess the enrichment levels of 29 immune-related functions between the two subsets. The results of ssGSEA analysis confirmed conspicuous differences between the two subsets (including APC co-stimulation, B-cells, APC co-inhibition, CCR, CD8⁺ T cells Checkpoint, Cytolytic activity, DCs, Mast cells, Neutrophils, HLA, iDCs, Macrophages, NK cells, T helper cells, pDCs, T cell co-inhibition, T cell co-stimulation, Parainflammation, Tfh, TIL, Type II IFN Response, Type I IFN Response, and Tregs) (Figure 7E). In addition, the relationship between 22 types of common infiltrated immune cells and 12 prognostic lncRNAs was highlighted through a correlation heatmap (Figure 7F). INC01094 displayed a distinct negative correlation with Plasma cells and B cells naive but positively correlated with macrophages M2.



The Importance of the NRLs-Based Signature in Chemotherapy and Immunotherapy

The IC50 values of 20 conventional chemotherapy agents in low-risk and high-risk subsets were calculated using the “pRRophetic” algorithm to assess the responses of STAD patients to chemotherapy. The two risk subsets had no statistically significant difference in their responses to the 16 chemotherapy agents but significantly different responses to the 4 anticancer drugs (**Figure 8A**). Moreover, patients in the low-risk subset were particularly sensitive to Cytarabine, which may be applied to SATD patients with a lower RS (**Figure 8B**).

The IC50 values of DMOG, Imatinib, and Sunitinib in the low-risk subset were higher, and these three drugs may be more applicable for patients with a higher RS based on the 12-NRLs signature (**Figures 8C–E**).

Given the significance of immune checkpoint inhibitor-based immunotherapy, the expression levels of five common immune checkpoint molecules (CD274, BTLA, CD28, CTLA4, and PDCD1LG2) between the low-risk and high-risk subsets were compared to evaluate the responses of STAD patients to immunotherapy. In comparison with STAD patients in the low-risk subset, five common immune checkpoint molecules had a higher expression in the high-risk subset, but the overexpression of CTLA4 was non-significant ($p = 0.075$).

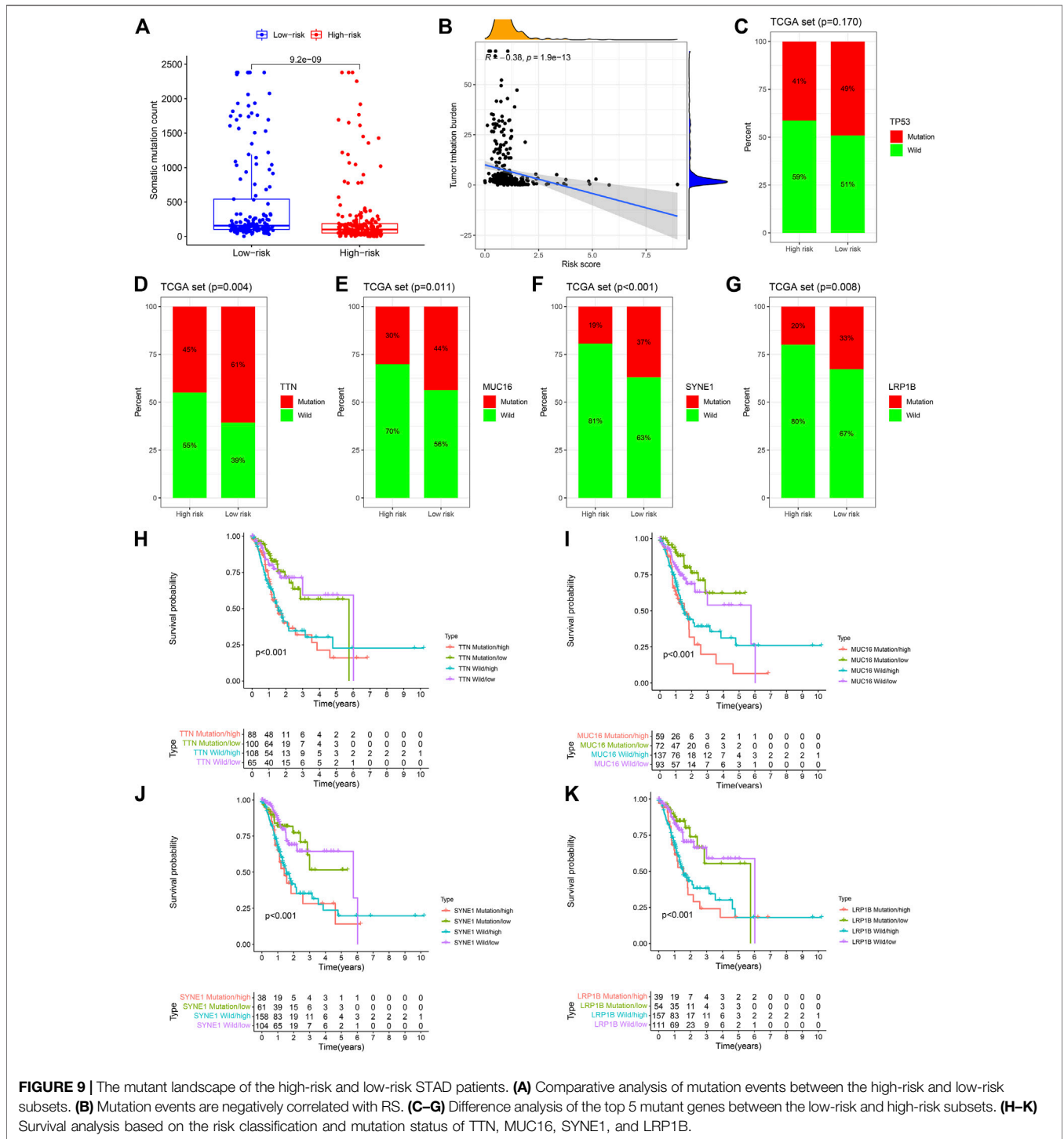


(Figure 8F–J). This indicated that STAD patients in the high-risk subset may up-regulate the expression of immune checkpoint genes to mediate immune evasion, which might confer patients’ unfavorable prognosis.

It was reported that TIDE algorithm can be applied to assess patient’ clinical response to ICI therapy. The higher the TIDE score, the greater the likelihood of immune escape, which might

mean more limited response to ICI therapy and the shorter survival time. To predict the clinical response to ICI therapy for STAD patients, TIDE analysis was carried out to evaluate the potential efficacy of immunotherapy in different risk subsets. Patients in the high-risk subset had higher TIDE, T cell exclusion, and T cell dysfunction score, indicating that STAD patients in the high-risk subset might

less likely to benefit from ICI therapy than in the low-risk subset (Figure 8K–M).

The Landscape of Somatic Gene Mutations Based on the 12-NRLs Signature

Given the significance of the tumor mutation burden (TMB) affecting the clinical responses of immune checkpoint inhibitors, information on somatic gene mutations of STAD patients was employed to investigate the correlations between TMB and RS. The detailed gene mutation information and regularity of STAD patients are presented in **Supplementary Figure S4**. Mutational events may be observed in the low-risk subset in comparison to the high-risk subset ($p < 0.001$) (Figure 9A). Spearman's correlation analysis revealed that RS had a significantly negative correlation to TMB (Spearman's correlation coefficient = -0.38) (Figure 9B). The mutational frequencies of the top 5 mutant genes between the low- and high-risk subsets were compared through the comparative mutation spectrum analysis (Figures 9C–G). Significant differences between the two risk subsets were observed in TTN, MUC16, SYNE1, and LRP1B. Then, based on the differential gene mutations and risk status, STAD patients were classified into four subsets according to these four genes to perform survival analysis. The subsequent results demonstrated that the OS of the four subsets corresponding to the four genes had significant differences ($p < 0.001$) (Figures 9H–K). The OS of patients in the TTN mutation/low-risk subset was longer than those in the TTN wild/high-risk subset. Similar results were also detected in the MUC16, SYNE1, and LRP1B, indicating that carrying wild-type genes was a hazard factor for the high-risk subset according to the 12-NRLs signature.

DISCUSSION

As a new type of strictly controlled cell death, necroptosis is mainly regulated by the activation of RIPK1 and RIPK3 and then executed by MLKL (phosphorylation, oligomerization, and membrane translocation), which eventually induces cell death (Cho et al., 2009; He et al., 2009; Zhang et al., 2009; Chen et al., 2014; Wang et al., 2014). Recent research has indicated that the role of necroptosis is paradoxical in anticancer-related biological processes (Zhu et al., 2019). On the one hand, necroptosis can be induced to play a considerable anticancer role when apoptosis is resisted. Smac mimetic can induce necroptosis in caspase-8-deficient colorectal cancer cells, thereby impeding the growth and proliferation of cancer cells in a mouse colorectal cancer model (He et al., 2017). Shikonin suppresses osteosarcoma progression *in vivo* by increasing the activity of necroptosis (Fu et al., 2013). Combining Smac mimetic Birinapant with caspase-8 inhibitor Emricasan can promote necroptosis in myeloid leukemia cells, which may emerge as a promising therapeutic method of AML (Brumatti et al., 2016). However, necroptosis of tumor cells can also facilitate cancer dissemination and metastasis. Necroptosis biomarkers are detected around the necrotic foci of breast cancer tissues in mice and humans, and necroptosis activity enhancement is involved in the aggravation of breast cancer progression and metastasis (Jiao et al., 2018). The

invasion and migration capability of head and neck squamous cell carcinoma (HNSCC) cells are enhanced by inducing necroptosis, the level of which is correlated with the survival of HNSCC patients (Li et al., 2020).

Considerable literature has focused on the effect of necroptosis on GC, while studies concerning the effects of NRLs are extremely lacking. Thus, investigating the prognostic value and molecular characteristics of NRLs in STAD is essential for the diagnosis and treatment of GC patients. In this study, NRLs were derived from the TCGA-STAD Transcript data using Pearson correlation analysis. Then, univariate analysis and LASSO regression analysis were employed to determine the most valuable NRLs for STAD prognosis. Eventually, 12 lncRNAs were selected to create the prognostic signature of necroptosis-associated lncRNAs (i.e., REPIN1-AS1, UBL7-AS1, LINC00460, LINC02773, CHROMR, LINC01094, FLNB-AS1, ITFG1-AS1, LASTR, PINK1-AS, LINC01638, and PVT1).

It has been reported that LINC00460 can enhance epithelial-mesenchymal transition (EMT) by promoting peroxidase-1 entrance into the nucleus in HNSCC (Jiang et al., 2019). Moreover, LINC00460 can silence CCNG2 to accelerate GC progression through EZH2/LSD1 epigenetics (Yang et al., 2020). LINC01094 has been demonstrated to enhance the invasion, migration, and EMT capabilities of ovarian cancer cells by adsorbing miR-577 (Xu et al., 2020). Additionally, LINC01094 also promotes the growth and metastasis abilities of glioblastoma cells through sponging miR-126-5p (Li and Yu, 2020). Furthermore, LASTR produced under stress can maintain and accelerate the growth of triple-negative breast cancer (TNBC) cells by regulating the activity of SART3 (De Troyer et al., 2020); PINK1-AS can facilitate Gai1-driven GC tumorigenesis through sponging microRNA-200a (Lv et al., 2021); LINC01638 is significantly upregulated in both NSCLC tissues and cells and regulated by the transcription factor SP1, which can enhance the proliferation of NSCLC cells and inhibit its apoptosis (Guo et al., 2019).

In order to demonstrate the practical value of the 12-NRLs signature, all STAD samples included were randomly distributed into the training and testing sets at a 1:1 ratio. The AUC values of ROC curves indicated that the signature had an acceptable predictive accuracy in both the training and testing sets (AUC = 1, 2, and 3 years reached 0.708, 0.732, and 0.748 in the training set; AUC = 0.658, 0.654, and 0.571 in the testing set). The signature proved broadly applicable and independent via Cox regression and stratified survival analysis. Calibration and DCA curves were plotted to confirm the predictive capability of the nomogram.

The immune cell infiltration in TME typically evolves along with tumorigenesis and development. In this study, samples in the high-risk subset had higher immune scores and lower levels of tumor purity based on TME scores. Further analysis revealed that the expression of T cells regulatory, macrophages M2, eosinophils, dendritic cells resting, and mast cells resting in the high-risk subset were significantly upregulated, indicating that these abnormal infiltrating immune cells may be correlated with STAD initiation and development. In particular, the infiltrated degree of immune-suppressive macrophages M2 and Tregs was positively correlated with RS, suggesting that the unfavorable

prognosis of patients in the high-risk subset may be partly due to the immunosuppressive microenvironment.

Chemotherapy and immunotherapy accompanied by surgery have become the primary approaches for GC. The sensitivity of 20 common chemotherapy agents in the low-risk and high-risk subsets were compared to guide clinicians in selecting appropriate anticancer drugs for STAD patients. Given the significance of immune checkpoint inhibitor-based immunotherapy, the discrepancies of five immune checkpoint blockade-related molecules between the low-risk and high-risk subsets were examined to assess the sensitivity of STAD patients to immunotherapy. The expressions of five common immune checkpoint molecules were higher in the high-risk subset, revealing that STAD patients in the high-risk subset may up-regulate the expression of immune checkpoint genes to mediate immune evasion, which might confer patients' unfavorable prognosis. TIDE score had been extensively applied to predict the therapeutic sensitivity with ICI treatment in many solid tumors. TIDE encompassed two underlying mechanisms of tumor immune escape: T cell dysfunction and T cell exclusion (Jiang et al., 2018). Patients in the high-risk subset had distinctly higher TIDE, T cell exclusion, and T cell dysfunction score, indicating that patients in the high-risk subset might possess more limited response to ICI therapy. In addition, TMB has been reported to predict the immunotherapy response of tumor patients (Rizvi et al., 2015; Chalmers et al., 2017). RS was found negatively correlated with TMB in this research, which may be associated with the immunological effects.

In short, the 12-NRLs signature was successfully created to predict the survival of STAD patients in this study. Additionally, investigating the molecular features based on the 12-NRLs risk signature was essential to expand new strategies and ideas for improving the therapy for STAD patients.

CONCLUSION

The 12-NRLs risk signature may help assess the prognosis and molecular features of STAD patients and improve the treatment modalities, which can be further applied clinically.

REFERENCES

- Bhan, A., Soleimani, M., and Mandal, S. S. (2017). Long Noncoding RNA and Cancer: A New Paradigm. *Cancer Res.* 77 (15), 3965–3981. doi:10.1158/0008-5472.can-16-2634
- Brumatti, G., Ma, C., Lalaoui, N., Nguyen, N. Y., Navarro, M., Tanzer, M. C., et al. (2016). The Caspase-8 Inhibitor Emricasan Combines with the SMAC Mimetic Birinapant to Induce Necroptosis and Treat Acute Myeloid Leukemia. *Sci. Transl. Med.* 8 (339), 339ra69. doi:10.1126/scitranslmed.aad3099
- Chalmers, Z. R., Connelly, C. F., Fabrizio, D., Gay, L., Ali, S. M., Ennis, R., et al. (2017). Analysis of 100,000 Human Cancer Genomes Reveals the Landscape of Tumor Mutational Burden. *Genome Med.* 9 (1), 34. doi:10.1186/s13073-017-0424-2
- Chen, J., Kos, R., Garssen, J., and Redegeld, F. (2019). Molecular Insights into the Mechanism of Necroptosis: The Necrosome as a Potential Therapeutic Target. *Cells* 8 (12). doi:10.3390/cells8121486

DATA AVAILABILITY STATEMENT

The datasets presented in this study can be found in online repositories. The names of the repository/repositories and accession number(s) can be found in the article/**Supplementary Material**.

AUTHOR CONTRIBUTIONS

LL research design and drafting the manuscript. LL literature search and helping to draft the manuscript. LL literature search and helping to draft the manuscript. ZF literature search and helping to draft the manuscript. QZ research design and drafting the manuscript. XS help modify articles and collate references. YC help modify articles and collate references. ZL review and revision of the manuscript and writing guidance.

FUNDING

This work was supported by the National Natural Science Foundation of China (No. 81860428), the Youth Science Foundation of Jiangxi Province (No. 20202BABL216051), the Science and Technology Plan of Health Commission of Jiangxi Province (No. 20191026), the Spark Promotion Plan of Grassroots Health Appropriate Technology of the Health Commission of Jiangxi Province (No. 68120198012), the Project of Science and Technology Department of Jiangxi Province (No. 20203BBGL73187), and the Traditional Chinese Medicine Research Project of Jiangxi Province (No. 2019A185), the Leading Talents Program of Jiangxi (20213BCJL22050).

SUPPLEMENTARY MATERIAL

The Supplementary Material for this article can be found online at: <https://www.frontiersin.org/articles/10.3389/fgene.2022.833928/full#supplementary-material>

- Chen, X., Li, W., Ren, J., Huang, D., He, W.-t., Song, Y., et al. (2014). Translocation of Mixed Lineage Kinase Domain-like Protein to Plasma Membrane Leads to Necrotic Cell Death. *Cell Res* 24 (1), 105–121. doi:10.1038/cr.2013.171
- Cho, Y., Challa, S., Moquin, D., Genga, R., Ray, T. D., Guildford, M., et al. (2009). Phosphorylation-driven Assembly of the RIP1-RIP3 Complex Regulates Programmed Necrosis and Virus-Induced Inflammation. *Cell* 137 (6), 1112–1123. doi:10.1016/j.cell.2009.05.037
- De Troyer, L., Zhao, P., Pastor, T., Baietti, M. F., Barra, J., Vendramin, R., et al. (2020). Stress-induced lncRNA LASTR Fosters Cancer Cell Fitness by Regulating the Activity of the U4/U6 Recycling Factor SART3. *Nucleic Acids Res.* 48 (9), 5198–5199. doi:10.1093/nar/gkaa280
- Declercq, W., Vanden Berghe, T., and Vandenabeele, P. (2009). RIP Kinases at the Crossroads of Cell Death and Survival. *Cell* 138 (2), 229–232. doi:10.1016/j.cell.2009.07.006
- Denaro, N., Merlano, M. C., and Lo Nigro, C. (2019). Long Noncoding RNA S as Regulators of Cancer Immunity. *Mol. Oncol.* 13 (1), 61–73. doi:10.1002/1878-0261.12413

- Feng, X., Song, Q., Yu, A., Tang, H., Peng, Z., and Wang, X. (2015). Receptor-interacting Protein Kinase 3 Is a Predictor of Survival and Plays a Tumor Suppressive Role in Colorectal Cancer. *Neoplasia* 62 (4), 592–601. doi:10.4149/neo_2015_071
- Ferlay, J., Colombet, M., Soerjomataram, I., Mathers, C., Parkin, D. M., Pineros, M., et al. (2019). Estimating the Global Cancer Incidence and Mortality in 2018: GLOBOCAN Sources and Methods. *Int. J. Cancer* 144 (8), 1941–1953. doi:10.1002/ijc.31937
- Fu, Z., Deng, B., Liao, Y., Shan, L., Yin, F., Wang, Z., et al. (2013). The Anti-tumor Effect of Shikonin on Osteosarcoma by Inducing RIP1 and RIP3 Dependent Necroptosis. *BMC Cancer* 13, 580. doi:10.1186/1471-2407-13-580
- Guo, L., Fang, L., and Liu, Y. (2019). SP1-regulated LINC01638 Promotes Proliferation and Inhibits Apoptosis in Non-small Cell Lung Cancer. *Eur. Rev. Med. Pharmacol. Sci.* 23 (20), 8913–8920. doi:10.26355/eurrev_201910_19287
- Guttman, M., and Rinn, J. L. (2012). Modular Regulatory Principles of Large Non-coding RNAs. *Nature* 482 (7385), 339–346. doi:10.1038/nature10887
- Hanson, B. (2016). Necroptosis: A New Way of Dying? *Cancer Biol. Ther.* 17 (9), 899–910. doi:10.1080/15384047.2016.1210732
- He, G.-W., Gunther, C., Thonn, V., Yu, Y.-Q., Martini, E., Buchen, B., et al. (2017). Regression of Apoptosis-Resistant Colorectal Tumors by Induction of Necroptosis in Mice. *J. Exp. Med.* 214 (6), 1655–1662. doi:10.1084/jem.20160442
- He, S., Wang, L., Miao, L., Wang, T., Du, F., Zhao, L., et al. (2009). Receptor Interacting Protein Kinase-3 Determines Cellular Necrotic Response to TNF- α . *Cell* 137 (6), 1100–1111. doi:10.1016/j.cell.2009.05.021
- Huarte, M. (2015). The Emerging Role of lncRNAs in Cancer. *Nat. Med.* 21 (11), 1253–1261. doi:10.1038/nm.3981
- Jiang, P., Gu, S., Pan, D., Fu, J., Sahu, A., Hu, X., et al. (2018). Signatures of T Cell Dysfunction and Exclusion Predict Cancer Immunotherapy Response. *Nat. Med.* 24 (10), 1550–1558. doi:10.1038/s41591-018-0136-1
- Jiang, Y., Cao, W., Wu, K., Qin, X., Wang, X., Li, Y., et al. (2019). lncRNA LINC00460 Promotes EMT in Head and Neck Squamous Cell Carcinoma by Facilitating Peroxiredoxin-1 into the Nucleus. *J. Exp. Clin. Cancer Res.* 38 (1), 365. doi:10.1186/s13046-019-1364-z
- Jiao, D., Cai, Z., Choksi, S., Ma, D., Choe, M., Kwon, H.-J., et al. (2018). Necroptosis of Tumor Cells Leads to Tumor Necrosis and Promotes Tumor Metastasis. *Cell Res* 28 (8), 868–870. doi:10.1038/s41422-018-0058-y
- Koo, G.-B., Morgan, M. J., Lee, D.-G., Kim, W.-J., Yoon, J.-H., Koo, J. S., et al. (2015). Methylation-dependent Loss of RIP3 Expression in Cancer Represses Programmed Necrosis in Response to Chemotherapeutics. *Cell Res* 25 (6), 707–725. doi:10.1038/cr.2015.56
- Li, J., Huang, S., Zeng, L., Li, K., Yang, L., Gao, S., et al. (2020). Necroptosis in Head and Neck Squamous Cell Carcinoma: Characterization of Clinicopathological Relevance and *In Vitro* Cell Model. *Cell Death Dis* 11 (5), 391. doi:10.1038/s41419-020-2538-5
- Li, X. X., and Yu, Q. (2020). linc01094 Accelerates the Growth and Metastatic-Related Traits of Glioblastoma by Sponging miR-126-5p. *Ott* 13, 9917–9928. doi:10.2147/ott.s263091
- Li, Y., Xiong, Y., Zhang, G., Zhang, L., Yang, W., Yang, J., et al. (2018). Identification of 5-(2,3-Dihydro-1h-Indol-5-Yl)-7h-Pyrrolo[2,3-D]pyrimidin-4-Amine Derivatives as a New Class of Receptor-Interacting Protein Kinase 1 (RIPK1) Inhibitors, Which Showed Potent Activity in a Tumor Metastasis Model. *J. Med. Chem.* 61 (24), 11398–11414. doi:10.1021/acs.jmedchem.8b01652
- Liu, L., Tang, Z., Zeng, Y., Liu, Y., Zhou, L., Yang, S., et al. (2021). Role of Necroptosis in Infection-related, Immune-mediated, and Autoimmune Skin Diseases. *J. Dermatol.* 48 (8), 1129–1138. doi:10.1111/1346-8138.15929
- Lv, Y., Wang, Y., Song, Y., Wang, S.-S., Cheng, K.-w., Zhang, Z.-q., et al. (2021). lncRNA PINK1-AS Promotes Gail-Driven Gastric Cancer Tumorigenesis by Sponging microRNA-200a. *Oncogene* 40 (22), 3826–3844. doi:10.1038/s41388-021-01812-7
- Marshall, K. D., and Baines, C. P. (2014). Necroptosis: Is There a Role for Mitochondria? *Front. Physiol.* 5, 323. doi:10.3389/fphys.2014.00323
- Molnár, T., Mázlo, A., Tslaf, V., Szollósi, A. G., Emri, G., and Koncz, G. (2019). Current Translational Potential and Underlying Molecular Mechanisms of Necroptosis. *Cell Death Dis* 10 (11), 860. doi:10.1038/s41419-019-2094-z
- Nugues, A.-L., El Bouazzati, H., Hétiuin, D., Berthon, C., Loyens, A., Bertrand, E., et al. (2014). RIP3 Is Downregulated in Human Myeloid Leukemia Cells and Modulates Apoptosis and Caspase-Mediated p65/RelA Cleavage. *Cell Death Dis* 5 (8), e1384. doi:10.1038/cddis.2014.347
- Rizvi, N. A., Hellmann, M. D., Snyder, A., Kvistborg, P., Makarov, V., Havel, J. J., et al. (2015). Cancer Immunology. Mutational Landscape Determines Sensitivity to PD-1 Blockade in Non-small Cell Lung Cancer. *Science* 348 (6230), 124–128. doi:10.1126/science.aaa1348
- Statello, L., Guo, C.-J., Chen, L.-L., and Huarte, M. (2021). Gene Regulation by Long Non-coding RNAs and its Biological Functions. *Nat. Rev. Mol. Cell Biol* 22 (2), 96–118. doi:10.1038/s41580-020-00315-9
- Strlic, B., Yang, L., Albarrán-Juárez, J., Wachsmuth, L., Han, K., Müller, U. C., et al. (2016). Tumour-cell-induced Endothelial Cell Necroptosis via Death Receptor 6 Promotes Metastasis. *Nature* 536 (7615), 215–218. doi:10.1038/nature19076
- Sung, H., Ferlay, J., Siegel, R. L., Laversanne, M., Soerjomataram, I., Jemal, A., et al. (2021). Global Cancer Statistics 2020: GLOBOCAN Estimates of Incidence and Mortality Worldwide for 36 Cancers in 185 Countries. *CA A. Cancer J. Clin.* 71 (3), 209–249. doi:10.3322/caac.21660
- Tan, Z. (2019). Recent Advances in the Surgical Treatment of Advanced Gastric Cancer: A Review. *Med. Sci. Monit.* 25, 3537–3541. doi:10.12659/msm.916475
- Wang, H., Sun, L., Su, L., Rizo, J., Liu, L., Wang, L.-F., et al. (2014). Mixed Lineage Kinase Domain-like Protein MLKL Causes Necrotic Membrane Disruption upon Phosphorylation by RIP3. *Mol. Cell* 54 (1), 133–146. doi:10.1016/j.molcel.2014.03.003
- Xu, J., Zhang, P., Sun, H., and Liu, Y. (2020). LINC01094/miR-577 axis Regulates the Progression of Ovarian Cancer. *J. Ovarian Res.* 13 (1), 122. doi:10.1186/s13048-020-00721-9
- Yang, J., Lian, Y., Yang, R., Lian, Y., Wu, J., Liu, J., et al. (2020). Upregulation of lncRNA LINC00460 Facilitates GC Progression through Epigenetically Silencing CCNG2 by EZH2/LSD1 and Indicates Poor Outcomes. *Mol. Ther. - Nucleic Acids* 19, 1164–1175. doi:10.1016/j.omtn.2019.12.041
- Zhang, D.-W., Shao, J., Lin, J., Zhang, N., Lu, B.-J., Lin, S.-C., et al. (2009). RIP3, an Energy Metabolism Regulator that Switches TNF-Induced Cell Death from Apoptosis to Necrosis. *Science* 325 (5938), 332–336. doi:10.1126/science.1172308
- Zhu, F., Zhang, W., Yang, T., and He, S.-d. (2019). Complex Roles of Necroptosis in Cancer. *J. Zhejiang Univ. Sci. B* 20 (5), 399–413. doi:10.1631/jzus.b1900160
- Zuo, J., Tao, M.-Q., Wu, X.-Y., Jiang, T.-T., Olatunji, O. J., Dong, J., et al. (2021). Securidaca Inappendiculata-Derived Xanthones Protected Joints from Degradation in Male Rats with Collagen-Induced Arthritis by Regulating PPAR- γ Signaling. *Jir* 14, 395–411. doi:10.2147/jir.s295957

Conflict of Interest: The authors declare that the research was conducted in the absence of any commercial or financial relationships that could be construed as a potential conflict of interest.

Publisher's Note: All claims expressed in this article are solely those of the authors and do not necessarily represent those of their affiliated organizations, or those of the publisher, the editors and the reviewers. Any product that may be evaluated in this article, or claim that may be made by its manufacturer, is not guaranteed or endorsed by the publisher.

Copyright © 2022 Luo, Li, Liu, Feng, Zeng, Shu, Cao and Li. This is an open-access article distributed under the terms of the Creative Commons Attribution License (CC BY). The use, distribution or reproduction in other forums is permitted, provided the original author(s) and the copyright owner(s) are credited and that the original publication in this journal is cited, in accordance with accepted academic practice. No use, distribution or reproduction is permitted which does not comply with these terms.